Journal of Power Sources 238 (2013) 218–226

Contents lists available at SciVerse ScienceDirect

Journal of Power Sources

journal homepage: www.elsevier.com/locate/jpowsour

Analysis of the dynamic performance of a microbial fuel cell using a system identification approach

Hitesh C. Boghani [a], Jung Rae Kim [a,1], Richard M. Dinsdale [b], Alan J. Guwy [b], Giuliano C. Premier [a,*]

[a] Sustainable Environment Research Centre (SERC), Faculty of Advanced Technology, University of Glamorgan, Pontypridd, Mid-Glamorgan, CF37 1DL, UK
[b] Sustainable Environment Research Centre (SERC), Faculty of Health, Sport and Science, University of Glamorgan, Pontypridd, Mid-Glamorgan, CF37 1DL, UK

HIGHLIGHTS

- We determine and consider validity of cause and effect models for a microbial fuel cell (MFC).
- We analyse the nonlinearity of the MFC by observing linear model parameters; variation with electrical loading.
- We show that MFCs subject to wide load variation can be modelled by piece-wise linearization.

ARTICLE INFO

Article history:
Received 20 July 2012
Received in revised form
26 February 2013
Accepted 11 March 2013
Available online 26 March 2013

Keywords:
Microbial fuel cell (MFC)
Bioelectrochemical system (BES)
System identification
Nonlinear system
Piece-wise linearisation
Parametric modelling

ABSTRACT

Microbial fuel cells (MFCs) are bioelectrochemical devices which use micro-organisms as catalyst for electrogenesis at the anode; oxidizing biodegradable substrate to produce electrical current. MFC power output is a function of many factors; including pH, temperature, loading rate, flow rate and electrical load. The study presents a system identification approach to determine a set of linear dynamic black box models able to quantify and represent specific nonlinear characteristics of a MFC. A sandwich-type MFC was subjected to varying electrical loads of various pseudo-random and step inputs, while observing the MFC voltage. Nonlinear behaviour was inferred from assumed piecewise linearised first order dynamic responses, at different operating points. The time constants increased from 0.5 s with PRBS loading of 100–150 Ω, to 6.2 s at 950–1 kΩ; although steady state gain varied little, (0.12–0.20 mV Ω^{-1}). This suggests that the MFC's non-linear behaviour, dependent on operating conditions, may be adequately represented by a series of linear models. System identification suggested that linear 4th order ARX models produce the best fit. However, reasonable prediction was observed using piecewise linearised first order models. The models could be used to design and optimize controllers to regulate power and/or voltage generation

1. Introduction

Growing global energy demands have provided drivers for technological developments to utilise renewable resources and mitigate growing greenhouse emissions. Among many other technologies, bioelectrochemical systems (BESs) can potentially contribute towards sustainable energy production and energy saving in waste treatment and other bioprocesses [1]. Microbial fuel cells (MFCs) as most BESs, utilizes anode respiring bacteria (ARB) as bio-catalysts, to generate electricity from biodegradable organic compounds including wastewater [1,2]. BES application to wastewater treatment and polishing, hydrogen production, electricity generation and biosensors has attracted researchers from many disciplines; e.g. recently Refs. [1,3–9]. A key ambition has been to increase the power production/performance and stability, and hence improve applicability of BESs.

MFCs are complex devices in so far as their bio-, physico- and electrochemical nature present highly coupled phenomena which represent the anodic biofilm and its interaction with the feedstock and system elements. They exhibit multiple dynamic processes; each affected by operating conditions such as temperature, pH, organic loading rate (OLR) and electrical load [10–12], amongst others. Therefore, identification of behaviour of MFC output due to such input(s) is of great interest in order to maintain optimized

* Corresponding author. Tel.: +44 (0)1443 482333; fax: +44 (0)1443 482169.
E-mail address: gcpremier@glam.ac.uk (G.C. Premier).
[1] Current address: School of Chemical and Biomolecular Engineering, Pusan National University, Busan 609-735, Republic of Korea.

0378-7753/$ – see front matter © 2013 Elsevier B.V. All rights reserved.
http://dx.doi.org/10.1016/j.jpowsour.2013.03.061

conditions. The electrical load is important in delivering maximum electrical power, as it affects the current drawn from the biofilm and can allow matching of external and internal impedance of the MFC/BES for maximum power transfer. These electrical signals, intrinsic to BES, can readily be employed to analyse MFC systems.

The performance of a MFC is expected to be nonlinear, as exemplified by the modelling of Picioreanu et al. [13] and the discussions of impedance presented by Zhao et al. [14]. Power and potential variations with load indicate that a single linear model will not represent a MFC over a range of operating load conditions. At the same time application of linear control strategies would be advantageous, and this paper considers the plausibility of modelling the system using a series of linear models in a piecewise linearisation methodology; assuming that performance over small perturbations [15] can reasonably be represented by a linear black box or process model. A series of such linear models may be scheduled according to applied load and model parameters may be interpolated between model instances, to represent the nonlinear dynamics of the MFC. While such an approach in a static form cannot account for time variation of the system, caused for example by changes in the biofilm, feed stock, temperature of other operating conditions; use of a system identification approach will allow for real-time estimation of model parameter by recursive identification methodologies [16,17]. This is particularly the case if the order and structure of the model do not change unpredictably with time. System modelling by identification has been applied to anaerobic reactors and various physical and chemical processes [18–21] and also 'conventional' fuel cells such as solid oxide fuel cells (SOFCs) [22–25], however this has not yet been the case in BES/MFCs. The utility of such modelling is expected to lie in providing suitable models for the development of control strategies.

Ha et al. [26] considered the time domain transient response of MFC potential to step change in load from very low (20 Ω) to very high (30 kΩ) to determine charge transfer resistance and the double layer capacitance. Ramasamy et al. [27] considered frequency domain characteristics to determine internal resistance of MFC using equivalent electrical circuit model. A resistance–capacitance (RC) network model of MFCs was reported by Montebelli et al. [28], as have several impedance models been determined by electrochemical impedance spectroscopy (EIS) e.g. Refs. [29–31]. Time variation has been investigated by EIS e.g. Ref. [29] and the particular considerations and concerns associated with electrochemical analyses of MFCs were elaborated in Ref. [31]. Stein et al. [32] have recently considered the identification of parameters in a linearised state-space model in order to represent the behaviour of their MFC based biosensor for detecting toxic components in the water. However, consideration of the cause/effect (electrical load to potential) non-linear dynamics of MFCs, over their whole operational load range, by piecewise linearisation has yet not been studied.

This study considers the dynamic cause and effect relationship which exists in BES, using MFC systems as a model process. Application of limited amplitude pseudo-random binary signal (PRBS) variations to the electrical load of a sandwich-type MFC was used to determine the dynamic relationship between electrical load and cell potential, which cannot be captured by static or near static measures such as the chrono-amperometrically, determined power and voltage against electrical load. In this study, we have shown for the first time that MFCs and by inference BES processes can reasonably be represented by linear models identified from data and that the models can represent the dynamic behaviour of the system over virtually the entire range of electrical load conditions. The piecewise linearised model might then be used to design systems for power and voltage control in BES, in order to regulate relative potentials and power recovery in stacks in real time, and to develop understanding of the dynamics of these systems, thus providing a further strategy for optimization and the prevention of system failures.

2. Materials and methods

2.1. MFC construction and operation

A MFC was constructed using carbon cloth anode (BASF Fuel Cell Inc., NJ, USA) with stainless steel woven wire mesh (size 70, 0.2 mm aperture) as current collectors (Mesh Direct, Burslem, UK), Cation Exchange Membrane (CMI-7000, Membrane International Inc., NJ, USA) and 5 mg cm^{-2} Pt coated carbon cloth cathode (BASF Fuel Cell Inc., NJ, USA) (Fig. 1a), sandwiched between Perspex sheets with 35 mm diameter and 10 mm thickness, leaving 9.6(+0/−1.0) mL of anodic volume as shown in Fig. 1b. The MFC was enriched using anaerobic sludge with acetate, phosphate buffer and nutrient media as previously described [33]. After enrichment, anodic fluid was discarded and replaced with fresh media with acetate (40 mM) and phosphate buffer and nutrient.

2.2. Application of PRBS input, step input and electrochemical analyses

An 8-bit pseudo-random binary signal (PRBS) was generated using LabVIEW™ and NI USB 2009 DAQCard™ (National Instruments, Newbury, UK) to produce a transistor–transistor logic (TTL) signal (0–5 V) to switch a relay (PVN012PbF, International Rectifier, CA, USA) through transistor array (ULN2003A, STMicroelectronics, Geneva, Switzerland). This effected switching between two levels of electrical load connected to MFC; with a PRBS minimum switching period $\Delta t = 5$ s. The resulting potential drop across the load was sampled at 0.5 s intervals (Fig. 2). PRBS electrical load

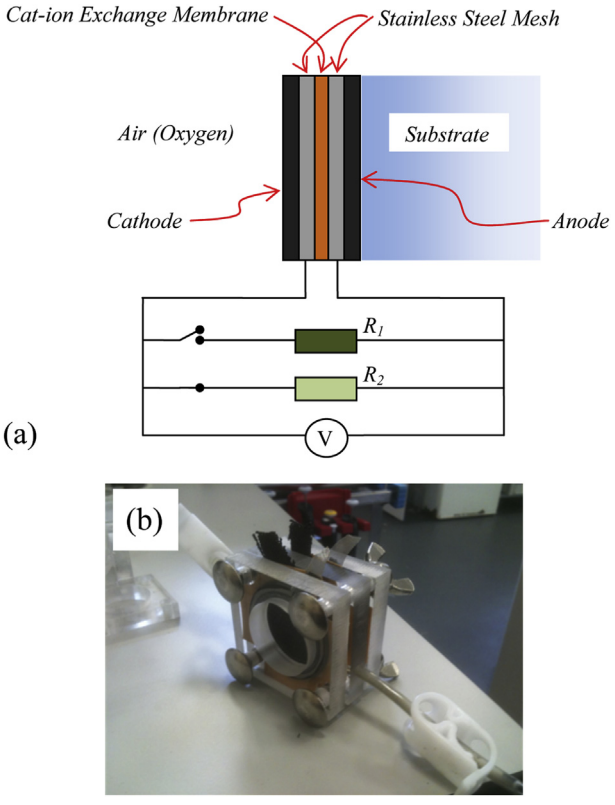

Fig. 1. (a) Schematic diagram of sandwich-type MFC under PRBS load, (b) sandwich-type MFC used in the study.

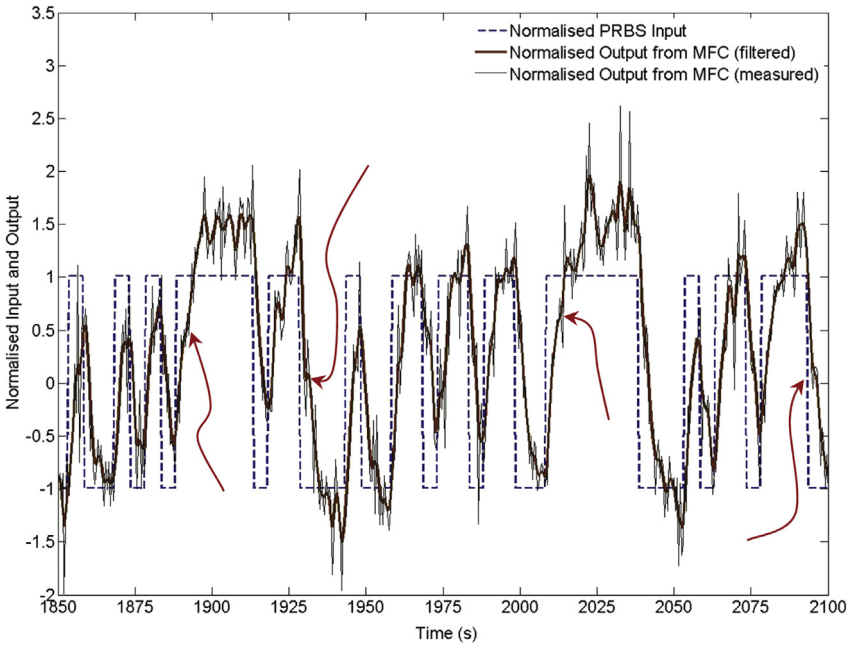

Fig. 2. A portion of normalised PRBS input (Ω) to the MFC and subsequent normalised output (V) from MFC. The portion is taken from PRBS loading of 804–851 Ω. The arrows show behaviour similar to the ones observed in Refs. [38,39] from MFCs.

modulation was applied with steps ranged from 100 Ω to 1 kΩ in 50 ± 5Ω intervals and steps of 1.7–2 kΩ and 4.4–5 kΩ. Load steps with higher amplitude in the latter two steps were selected to compensate for very low static gain for the linear models at higher loading.

MFCs were also subjected to step inputs ranging from 100 Ω to 1 kΩ in 50 Ω resistance intervals using resistance decade box (Resistance Decade Box, TENMA, Japan) and voltage development was observed.

The power variation with current was determined by decreasing the electrical load from 50 kΩ to 200 Ω in steps while measuring the voltage. The resistance was changed after the voltage was seen to have settled (steady-state). The electrical current and power were calculated using $I = V/R$ and $P = V^2/R$, respectively where, I is electrical current (A), P is power (W), V is voltage (V) and R is electrical load (Ω). Power density (W m^{-3}) was calculated using an empty anodic chamber volume of 9.6 mL.

2.3. Mathematical analyses

The cause (electrical load)/effect (potential drop) or input/output data obtained from experiments were visually inspected for outliers and trends before identification proceeded. In each data sets with PRBS loading of 150–200 Ω, 650–700 Ω and 855–900 Ω (less than 0.07% of samples were outliers), which were considered to be related to disturbances to electrical connections and were removed and replaced with the mean of previous and subsequent sample values either side of the outlier. Some trends caused by substrate depletion were also found in the PRBS data after relatively long periods of operation and/or at substrate addition. Trends and offsets were removed by using a *DETREND* function available in MATLAB® (The MathWorks, Inc., Cambridge, UK) to remove linear trends in the data and signal offsets by subtracting sample means from the signals. The data were normalised as previously described by Premier et al. [21] and were subsequently imported to a System Identification Toolbox™ (The Mathworks, Inc.) environment for identification. The data so obtained was then split to provide separate data for parameter estimation (estimation data) and model validation (validation data).

Process models of the general transfer function form (1st order) were considered, informed by *a priori* knowledge from step responses as shown in Eq. (1):

$$\frac{V_o}{R_i} = \frac{k}{1 + T_p \cdot s}, \tag{1}$$

where V_o is voltage output in volts, R_i is load input in ohms and s is the Laplace variable. The parameters, steady-state gain, k (mV Ω^{-1}); time constant, T_p (s) were determined at several operating points.

Single Input Single Output (SISO) AutoRegressive with eXtra inputs (ARX) models of the general form previously described by Premier et al. [21] were also considered for the PRBS data corresponding to PRBS loading of 200.6–250.4 Ω onwards. An iterative estimation algorithm to estimate the parameters of the process models using the minimising prediction-error method [34], as implemented in the System Identification Toolbox™, MATLAB®. For the ARX structure, a least squares estimation method [34] was likewise employed. The data for PRBS loading of 804–851 Ω was also split in four equal parts; each part to be considered for the identification separately. Validation of models was considered through analysis of residuals, simulation of step responses and comparison of simulated model responses against validation data subject to the same PRBS input, as described by Ljung [35].

Responses to the step inputs applied to the MFC (Fig. 3), the time constants τ and steady-state gains K were determined, assuming 1st order system dynamics with no time delay. The MFC output potentials were simulated using parameters obtained from the step responses, using Eq. (2):

$$V_o(t) = R_i \cdot K\left[1 - \exp\left(-\frac{t}{\tau}\right)\right], \tag{2}$$

where, $V_o(t)$ is voltage (output) at time t and, R_i is the load resistance (input). For step responses, K is steady-state gain and τ is the time constant in seconds.

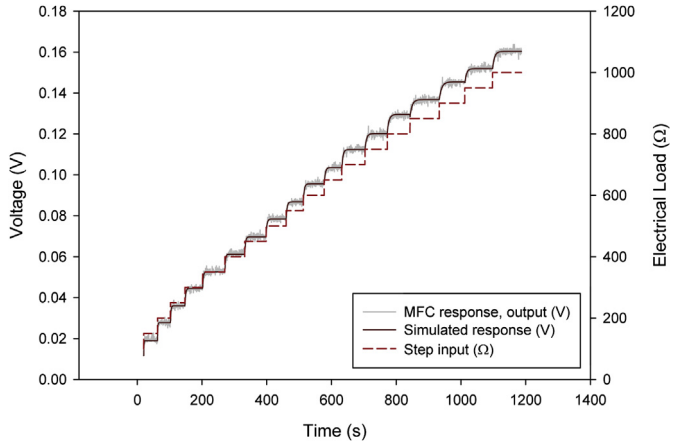

Fig. 3. Assuming 1st order process, MFC step responses and simulated step responses from parameters determined from MFC response (V) to step input (Ω).

3. Results

3.1. MFC performance and step responses

The power curve of the MFC was measured to determine the operational range (cell potential) with associated power levels resulting from variations in electrical loading, amongst other operational parameters such as substrate concentration (40 mM sodium acetate), pH (7.0) and temperature (30 °C) being constant. Power and voltage curves are plotted against electrical load on a logarithmic scale ($\log_{10}$) to reduce the spread of data, as shown in Fig. 4a. When electrical load (connected to the MFC) was varied from 50 kΩ to 200 Ω, potential drop across the load varied from 0.415 V to 0.037 V, producing a peak power of 3.26 W m^{-3} at 2 kΩ.

In order to assess the transient behaviour of the cell potential from MFC, several step changes in load resistance R_i were applied, within the range 100 Ω to 1 kΩ (Fig. 3). Estimated time constants, τ and steady-state gains, K (which together define linear 1st order dynamics), were determined from the step response data, and are presented in Fig. 4b. It can be seen that the time constants increase gradually from 0.5 s to 7.3 s as load resistance is increased in steps of 50 Ω from 150 Ω to 1 kΩ. Steady-state gains varied from 0.12 to 0.20 mV Ω^{-1} over the same range.

3.2. System identification and validation

The MFC was perturbed with PRBS load variations from relatively low load resistances of 100 Ω up to relatively high loads of 5 kΩ covering the whole operational range of MFC. A portion of the PRBS load input variations and consequent MFC voltage output illustrates typical PRBS data recorded (Fig. 2). The portion of input–output data presented in Fig. 2 are in their normalised form corresponding to PRBS loading of 804–851 Ω. The output data were filtered using a 5th order Butterworth filter as used by Premier et al. [21] and is presented in Fig. 2 in order to visually assess transient behaviour of the MFC. However, raw data were used for the identification process. The linearised models were identified and are presented with 1st order process models and 4th order ARX model structures.

Parameters estimated from PRBS data, employing 1st order process models (Eq. (1)), are presented in Fig. 4b. Estimated time constants (T_p) gradually increased from 0.7 s to 6.2 s as PRBS loading was varied from relatively lower loading of 100–150 Ω to relatively higher loading of 950–1 kΩ. Time constants at PRBS loading of 1.7–2 kΩ and 4.4–5 kΩ were estimated to be 4.9 s and

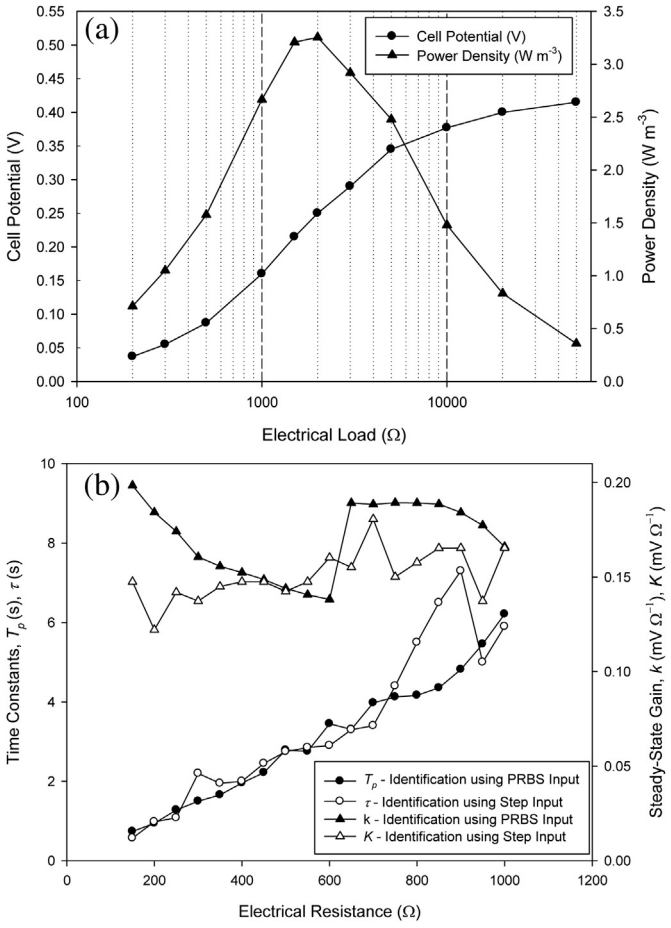

Fig. 4. (a) Power density and cell potential as function of electrical load for MFC used in the study. The abscissa is represented in $\log_{10}$ scale. (b) Assuming 1st order-type response from MFC, comparison of time constants (τ,T_p) and steady state gains (K,k) obtained from system identification using step input and PRBS input.

12.3 s (data not shown), respectively. Estimates of steady-state gains (k) varied from 0.14 mV Ω^{-1} to 0.20 mV Ω^{-1} with the range of PRBS loading between 100 Ω and 1 kΩ. Steady-state gains were determined to be 0.175 mV Ω^{-1} and 0.091 mV Ω^{-1} for PRBS loading of 1.7–2 kΩ and 4.4–5 kΩ (data not shown), respectively. Time constants and steady state gains for split data sets (4 sets out of 1 experimental run) from PRBS loading of 804–851 Ω varied from 4.8 s to 5.1 s and 0.187 mV Ω^{-1} to 0.189 mV Ω^{-1} (data not shown).

Parameters estimated from identification for ARX models are presented in Table 1 as per the general form of transfer function shown (in z-domain) in Eq. (3):

$$\frac{V_o}{R_i} = \frac{K\cdot(z-z_1)(z^2-z_b\cdot z+z_c)}{(z-p_1)(z-p_2)(z^2-p_b\cdot z+p_c)}, \quad (3)$$

where K is steady-state gain, z_1 is zero, p_1 and p_2 are poles, z_b, z_c, p_b, p_c are coefficients of quadratic form of zero and pole terms.

Analyses of residuals (the difference between predicted output and measured output from validation data sets) were performed on each identification sets to investigate the confidence limits (95%) of auto and cross-correlations (Fig. 5a–c). Autocorrelation performed on residuals should show correlation only when residuals have no relative temporal delays. The autocorrelation function within the 95% confidence levels indicates that the residuals and model output are un-correlated and lends validity to the model and are shown in Fig. 5a. Cross-correlation was performed between residuals and the

Table 1
Parameters of 4th order ARX model transfer function and model fits (%) for ARX and process models from validation.

PRBS Loading	K ($\times 10^{-4}$)	z_1	z_b	z_c	p_1	p_2	p_b	p_c	Model fit (ARX) %	Model fit (process[a]) %
101.2–150.4 Ω	–	–	–	–	–	–	–	–	–	44.08
151.5–200.5 Ω	–	–	–	–	–	–	–	–	–	41.57
200.6–250.4 Ω	1.67	−0.38	0.02	0.12	0.70	−0.51	−0.12	0.25	77.54	76.76
250.8–301.6 Ω	1.54	−0.51	0.12	0.17	0.73	−0.47	−0.19	0.28	77.23	76.30
302–351.5 Ω	1.50	−0.04	−0.26	0.15	0.77	−0.55	−0.10	0.33	73.38	73.38
352.2–400.7 Ω	1.47	0.39	−0.68	0.49	0.82	−0.43	−0.20	0.24	75.13	74.80
402.6–450.5 Ω	1.44	−0.15	−0.18	0.14	0.81	−0.55	−0.11	0.32	71.89	71.31
452.7–500.3 Ω	1.39	0.12	−0.52	0.29	0.83	−0.54	−0.10	0.33	67.76	66.69
503.1–550.3 Ω	1.37	0.19	−0.57	0.27	0.84	−0.51	−0.13	0.32	64.22	63.75
553.2–600.2 Ω	1.35	0.13	−0.59	0.27	0.84	−0.52	−0.18	0.32	64.24	62.54
602.5–650.1 Ω	1.83	−0.43	0.01×10^{-3}	0.10	0.86	−0.47	−0.20	0.37	64.59	64.01
652.7–701.3 Ω	1.84	−0.60	0.24	0.14	0.86	−0.59	−0.06	0.33	71.40	70.68
704–751.3 Ω	1.85	−0.07	−0.54	0.19	0.87	−0.60	−0.09	0.38	71.16	70.80
754.7–802 Ω	1.85	−0.27	−0.24	0.17	0.88	−0.51	−0.20	0.38	69.89	70.06
804–851 Ω	1.85	0.18	−0.60	0.36	0.89	−0.58	−0.11	0.34	67.52	66.51
804–851 Ω (part 1 of 4)	1.85	0.39	−1.43	0.81	0.91	−0.66	−0.01	0.32	65.70	64.79
804–851 Ω (part 2 of 4)	1.85	0.31	−0.56	0.40	0.88	−0.60	−0.16	0.34	66.61	64.79
804–851 Ω (part 3 of 4)	1.85	−0.52	0.36	0.34	0.87	−0.61	−0.07	0.40	67.59	67.81
804–851 Ω (part 4 of 4)	1.85	−0.44	0.24	0.34	0.87	−0.52	−0.21	0.34	66.73	63.05
855–901 Ω	1.80	−0.57	0.04	0.19	0.89	−0.55	−0.23	0.37	62.19	61.81
904–951 Ω	1.74	−0.42	−0.16	0.41	0.87	−0.59	−0.12	0.38	57.14	58.18
954–1 kΩ	1.62	−0.44	−0.02	0.33	0.89	−0.60	−0.12	0.40	53.06	52.84
1.7–2 kΩ	1.73	0.83	−0.66	0.38	0.91	−0.59	−0.04	0.34	53.10	30.11
4.4–5 kΩ	0.90	−0.63	0.42	0.12	0.81	−0.62	−0.07	0.36	30.99	21.48

[a] Parameters for process models are presented in Fig. 4 for PRBS loading of up to 1 kΩ. Time constant, T_p and steady-state, k gain are 4.9 s (12.3 s) and 0.175 mV Ω^{-1} (0.091 mV Ω^{-1}) for PRBS loading of 1.7–2 kΩ (4.4–5 kΩ).

normalised inputs. The cross-correlation function within the 95% confidence interval levels indicates that the residuals are uncorrelated to the input.

For each model identified from PRBS data, its response to a unit step input was simulated to examine the transient step responses of identified models and an example is plotted in Fig. 6 for PRBS loading of 352.2–400.7 Ω. From validation data sets, the time-series normalised output was simulated and predicted using the identified process models and ARX models, respectively. The data were plotted along with the validation data sets to see if the model output matches the measured output. The best fit (in %) of model response to the actual response data in validation data set was determined using Eq. (4) [35] and is presented in Table 1 for all identified models.

$$\text{Best fit}(\%) = \left(1 - \frac{|y - \hat{y}|}{|y - \bar{y}|}\right) \times 100. \quad (4)$$

Here, y is measured output, $\hat{y}$ is the model output and $\bar{y}$ is the mean of measured output. An example of such validation for PRBS loading of 804–851 Ω is shown in Fig. 7 with best fit of 66.51% and 67.52% for the process model and ARX model, respectively.

4. Discussion

4.1. Steady-state gain and time constants

In applying MFCs and BESs to wastewater treatment and waste streams, it is likely that high current densities will be beneficial as COD removal through electrogenic metabolism is directly related to the current density. Controlling cell potential and power delivery from MFCs/BESs will be important as it can benefit from identified models by facilitating controller design; particularly as the models may be inferred and controllers adapted in real-time by employing well established recursive algorithms. Identified models may be used in system design and analysis for which their dynamic behaviour is of interest and can be identified over their entire operational range.

Identified MFC models were linearised about a range of operating points by applying small perturbation theory and the MFC behaviour was found to be reasonably described by a 1st order linear differential equation/process model (transfer function). No input-to-output time delays of significance were detected, with the enriched MFC responses starting almost instantaneously at the application of step load changes. The steady-state gain (k) estimated at different operating load conditions (Fig. 4b) varied between 0.12 and 0.20 mV Ω^{-1}. Hence steady state gain varied by only ~4 mV for a 50 Ω step change, throughout the range 100 Ω to 1 kΩ. For the step change in load from 4.4 kΩ to 5 kΩ, the steady-state gain was 0.091 mV Ω^{-1}, which is much lower than at the lower external loads. PRBS loading was therefore not carried out in the higher loading (i.e. lower current) range. The voltage curve in this region of higher loading is relatively flat and hence changes in load have limited effect on voltage. It is seen that the voltage increase is almost linearly proportional to the increase in load in the range of 200 Ω to 2 kΩ (Fig. 4a). Voltage then starts to deviate and saturate at higher loads as the internal resistance of the MFC becomes less significant compared to a very high external load (tending to open circuit) and the voltage drop across the external load approaches the open circuit potential of the MFC [36].

The time constant increased in a smooth manner from 0.5 s to 7.3 s over the range of applied electrical loads (150 Ω to 1 kΩ). The system dynamics, i.e. speed of response, slowed and became more dominant as the system approached maximum power point (Fig. 4a and b). Substantial increase in time constant with increase in external load (operational point) confirms that the MFC system is nonlinear. Such nonlinearity and change in model parameter (time constant) would have to be considered when designing a controller to control MFC as the controller designed for high current region (small time constant) would not be adequate for relatively lower current region (large time constant). However, linear process models (and also linear ARX models) identified in this study indicate that piece-wise linearisation of the MFC system is possible and

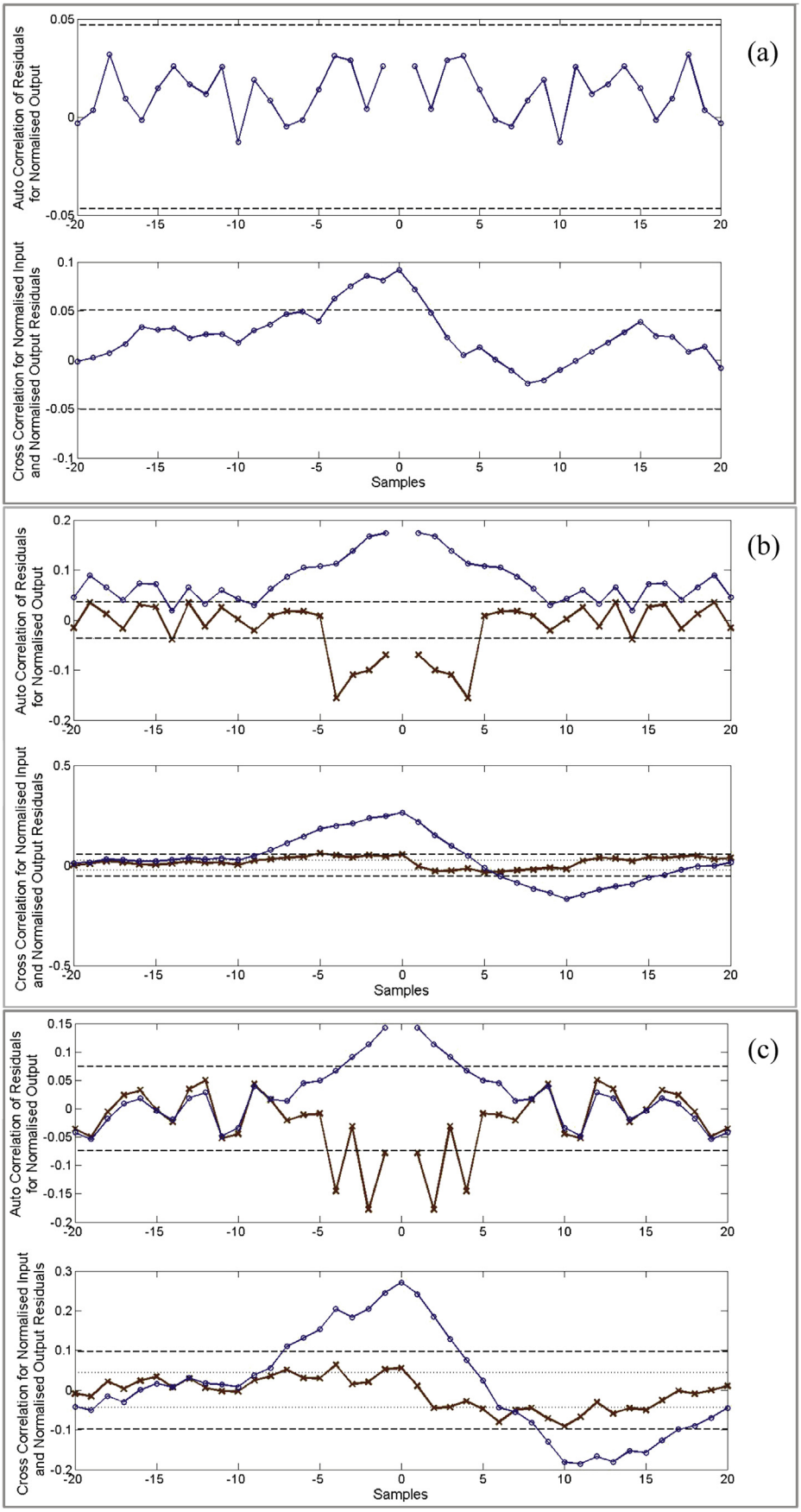

Fig. 5. Autocorrelations and cross-correlations on system identification validation data for PRBS loading of (a) 151.5–200.5 Ω; (b) 804–851 Ω; and (c) 804–851 Ω (1/4th portion of PRBS data). Curves on the graph are ····· (ARX) 95% Confidence Interval +, ····· (ARX) 95% Confidence Interval −, — — — (Process) 95% Confidence Interval +,— — — (Process) 95% Confidence Interval −, —o— Process Model and —x— ARX Model.

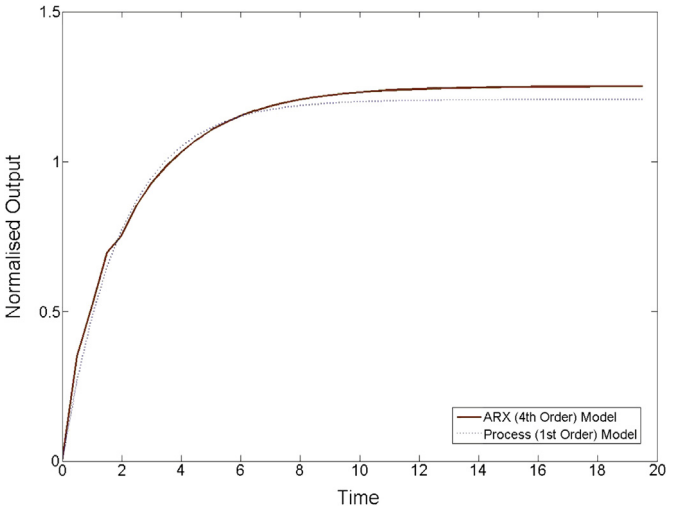

Fig. 6. Simulated normalised output to a unit step input using models obtained from system identification of PRBS loading of 352.2–400.7 Ω.

that the MFC could be represented over a wide range of loading, by a series of linear models to be plausibly used in control.

In comparing time constants obtained from step response analyses and process model identification (Fig. 4b), good agreement is found in the loading range of 100 Ω to 800 Ω. However, there is some divergence in the region of 800–950 Ω. Prolonged perturbation from the applied PRBS, could have affected the anodic biofilm, resulting in a more responsive system with shorter time constants than experienced with single steps.

The black box (ARX) models of MFCs, while not representing the underlying processes, may nevertheless find utility in the design of control strategies. Linear control may suffice within a narrow operating range, but would require adaption to operate over a wider operating range. Therefore, the models identified at different operating levels provide useful dynamic information enabling appropriate controller parameterisation for use in adaptive control e.g. gain scheduling [37], enabling optimal MFC control throughout the operating range.

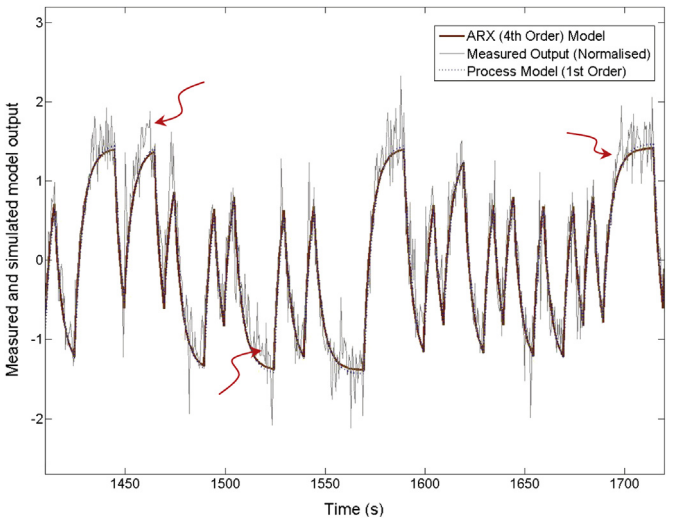

Fig. 7. Measured and simulated model output for PRBS loading of 804–851 Ω with ARX model of 4th order and process model of 1st order (validation). The arrows indicate random deviation of MFC output from anticipated rise and fall curves.

4.2. Model validation and analyses of residuals

The validity of the models identified was examined through the residuals (errors between simulated model outputs) and model validation output data. Autocorrelations of residuals from process models structure, subject to PRBS loading of up to 200.5 Ω, were typically found to be within 95% confidence level (an example for 151.5–200.5 Ω is shown in Fig. 5a). This suggests that by this measure, the process model described the observed dynamic behaviour of the MFC to a relatively high level (95%) of confidence. However, for PRBS load perturbation alternating between 250.8 Ω and 301.6 Ω and higher loads, the autocorrelation function did not meet the 95% confidence level, as illustrated in Fig. 5b for the PRBS loading of 804–851 Ω, indicating that the dynamics represented by the validation data set were not well represented by the 1st order process model. A higher (3rd) order process model was also considered, but did not improve the autocorrelation (data not shown). A linear ARX model of 4th order was considered as an alternative to the process model structure and improved the autocorrelation function, which is shown in Fig. 5b. The 4th order simulated unit step response (normalised output) of the ARX model shown in Fig. 6 can be seen to present an approximation to a 1st order step response and the autocorrelations performed on residuals for the ARX models were found to be reasonably within the 95% confidence limits.

The validation revealed that in some parts (indicated by arrows in Fig. 7) the output from MFC deviated noticeably but randomly from the estimated model response as steady-state approached which was thought to have an impact on autocorrelations and were not explained by the model. Autocorrelation functions for both, process and ARX models from identification of split data sets from PRBS loading of 804–851 Ω were within 95% confidence interval one of which is shown in Fig. 5c. Also, time constants (~5 s) and steady state gains (~0.19 mV Ω^{-1}) obtained for process models were similar to the ones obtained from identification from original data set. It is clear that as the MFC was subject to higher external loads, the dynamic response became slower. However, the voltage output sampling times were not altered to compensate for the slower dynamics. As a result, the voltage fluctuations due to noise became significant in the correlation analyses. To improve model validation by residual analyses, slower sampling time should be considered in line with slower dynamics exhibited by MFCs at higher loads.

The cross-correlation function for PRBS loading of 151.5–200.5 Ω was within the 95% confidence interval except for the limited lag (sample) range of 1 to −4. For PRBS loading of 804–851 Ω, the cross-correlation function lies outside the confidence limits at several points for both, process and ARX models. Fig. 2 suggests an oscillatory output from the MFC, which is more clearly seen in the filtered signal which appears as cyclic in the cross-correlations (Fig. 5). However, visual inspection of simulation-validation data and data fit collectively as shown in Fig. 7 and Table 1 suggests that the models reasonably represent the observed data.

4.3. Order of the system and its implications

The MFC tested exhibited behaviour, as indicated by the arrows in Fig. 2, that might be considered to represent a dominant first order pole along with a pair of less dominant complex poles producing an oscillatory response and a zero, together approximating a 1st order dynamic; when superimposed onto the characteristic exponential rise of a 1st order system subject to a step response. Ignoring the noise and complex poles (which may be an artefact of the filter and noise), this behaviour from MFC accords with earlier

studies, e.g. the response to change in electrical load from 1 Ω to open circuit presented by Cheng et al. [38] who relate the response to the anodic biofilm's affinity to an electrode potential (−420 mV vs Ag/AgCl for an acetate consuming MFC) which represents saturation of anode respiring bacteria. The approximately 1st order dynamics are also evident in response to step changes in organic loading rate as presented by Kim et al. [39].

The PRBS based process identification at lower loading, assumed 1st order responses which was shown to be reasonable through the simulation and autocorrelation function presented previously. However, as loading increased, oscillations in the output progressively increased and became significant and more pronounced as maximum power point was approached (filtered signal in Fig. 2). This suggests that though MFC responses tend to 1st order, the system order may alter and increase towards peak power conditions. Biofilms in MFCs are frequently dominated by *Geobacter* spp. as suggested by Logan and Regan in relation to ARBs [40]. Also, studies by Richter et al. [41] have shown that cytochromes such as OmcS and OmcZ support attachment and transport electrons (through redox reactions between cytochromes) from bacteria to anode electrode. Bonanni et al. [42] suggest that in MFCs with *Geobacter sulfurreducens* biofilms, the electron transfer process from oxidation of acetate to the anode electrode, considering a transport chain including internal cytochromes and a matrix of dermal cytochromes within the biofilm and biofilm–electrode interface; is limited by the microbial uptake of acetate and transfer of electrons to cytochromes rather than the cytochromal processes, which are suggested to be much faster (approx. 11 times) [42]. It is possible that the non-minimum phase effect presented and ascribed to cytochrome behaviour by Bonanni et al. [42], is indicative of a nonlinear behaviour and an interplay between the faster and slower dynamic systems may appear as oscillatory higher order dynamics in the identification process. Also, MFCs are dependent on variables such as pH, temperature, substrate concentration, electrode kinetics, proton transport through the ion exchange membrane, substrate oxidation and electron transport chain, electrical current, oxygen diffusion to cathode electrode and their interactions among. Haldane-like kinetics or other nonlinearities may also lead to oscillatory or higher order behaviours when piece-wise linearised. Identification at high power conditions suggests that the MFC system could better be represented by a 4th order transfer function. MFCs typically have predictable outputs (Fig. 7) and to avoid unnecessary complexity, order reduction should be considered. 1st order representation is comparatively suitable in representing validation data, showing little advantage from a higher 4th order model, as seen in Fig. 7, with best fit % indicated in Table 1.

So, the MFC/BES linear models identified here could be scheduled for appropriate loading range to model voltage (current or power) output; providing the intrinsic parameters such as anodic biofilm, materials, solution conductivity, etc. do not change significantly with time. Recursive identification could be employed to track changes in parameters in real-time. Control strategies employing adaptive methods could avoid voltage reversal in MFC stacks and could improve system performance.

5. Conclusion

The MFC system is a nonlinear process which presents slower dynamic behaviour as maximum power point is approached. System identification tools were found to be applicable to these systems. Parameter estimation applied to alternative model structures was investigated across a wide range of electrical loads applied to a MFC as an exemplar for BES.

The MFC tested could reasonably be represented by a series of linear input–output process models of 1st order structure, for most input electrical load conditions. However, the system was better represented by ARX model structures at loads which represented the region of peak power operation. Although, a 4th order ARX model provided the best fit to validation data, it is likely that lower order models will adequately represent the process for practical purposes. So, it is possible to identify a piecewise linearised model over a range of operating conditions, by assembling a series of linear models which are scheduled (or used) at the appropriate operating conditions.

Acknowledgement

This research was funded by the RCUK Energy Programme, SUPERGEN Biological Fuel Cell project (EP/D047943/1) supported by grant 68-3A75-3-150. The Energy Programme is an RCUK cross-council initiative led by EPSRC and contributed to by ESRC, NERC, BBSRC and STFC.

References

[1] S.T. Oh, J.R. Kim, G.C. Premier, T.H. Lee, C. Kim, W.T. Sloan, Biotechnology Advances 28 (2010) 871–881.
[2] B. Logan, B. Hamelers, R. Rozendal, U. Schroder, J. Keller, S. Freguia, P. Aelterman, W. Verstraete, K. Rabaey, Environmental Science & Technology 40 (2006) 5181–5192.
[3] N. Yoshida, H. Nakamura, I. Karube, K. Yano, T. Morita, S.J. McNiven, The Analyst 125 (2000) 2280–2284.
[4] I.S. Chang, J.K. Jang, G.C. Gil, M. Kim, H.J. Kim, B.W. Cho, B.H. Kim, Biosensors and Bioelectronics 19 (2004) 607–613.
[5] L. Zhuang, Y. Zheng, S. Zhou, Y. Yuan, H. Yuan, Y. Chen, Bioresource Technology 106 (2012) 82–88.
[6] K.P. Katuri, K. Scott, Biotechnology and Bioengineering 107 (2010) 52–58.
[7] Z. Du, H. Li, T. Gu, Biotechnology Advances 25 (2007) 464–482.
[8] M.F. Manuel, V. Neburchilov, H. Wang, S.R. Guiot, B. Tartakovsky, Journal of Power Sources 195 (2010) 5514–5519.
[9] M. Sun, G.-P. Sheng, Z.-X. Mu, X.-W. Liu, Y.-Z. Chen, H.-L. Wang, H.-Q. Yu, Journal of Power Sources 191 (2009) 338–343.
[10] G.S. Jadhav, M.M. Ghangrekar, Bioresource Technology 100 (2009) 717–723.
[11] I.S. Michie, J.R. Kim, R.M. Dinsdale, A.J. Guwy, G.C. Premier, Energy & Environmental Science 4 (2011) 1011.
[12] X.-C. Zhang, A. Halme, Biotechnology Letters 17 (1995) 809–814.
[13] C. Picioreanu, I.M. Head, K.P. Katuri, M.C.M. van Loosdrecht, K. Scott, Water Research 41 (2007) 2921–2940.
[14] F. Zhao, N. Rahunen, J.R. Varcoe, A.J. Roberts, C. Avignone-Rossa, A.E. Thumser, R.C.T. Slade, Biosensors and Bioelectronics 24 (2009) 1931–1936.
[15] H.K. Khalil, Nonlinear Systems, Prentice Hall, 2002.
[16] P.C. Young, Journal of Forecasting 30 (2011) 104–146.
[17] H.P. Wang, B. Kalchev, Y. Tian, I. Simeonov, N. Christov, C. Vasseur, in: 2011 19th Mediterranean Conference on Control & Automation (MED) (2011), pp. 1140–1143.
[18] I. Gustavsson, Automatica 11 (1975) 3–24.
[19] K. Kristinsson, G.A. Dumont, in: IEEE Transactions on Systems, Man and Cybernetics, vol. 22, 1992, pp. 1033–1046.
[20] K.C. Tan, Y. Li, D.J. Murray-Smith, K.C. Sharman, in: Genetic Algorithms in Engineering Systems: Innovations and Applications, 1995. GALESIA. First International Conference on (Conf. Publ. No. 414) 1995, pp. 164–169.
[21] G.C. Premier, R. Dinsdale, A.J. Guwy, F.R. Hawkes, D.L. Hawkes, S.J. Wilcox, Water Research 33 (1999) 1027–1037.
[22] F. Jurado, Journal of Power Sources 129 (2004) 205–215.
[23] F. Jurado, Fuel Cells 5 (2005) 105–114.
[24] F. Jurado, Journal of Power Sources 158 (2006) 245–253.
[25] F. Jurado, Journal of Power Sources 154 (2006) 145–152.
[26] P.T. Ha, H. Moon, B.H. Kim, H.Y. Ng, I.S. Chang, Biosensors and Bioelectronics 25 (2010) 1629–1634.
[27] R.P. Ramasamy, Z. Ren, M.M. Mench, J.M. Regan, Biotechnology and Bioengineering 101 (2008) 101–108.
[28] A. Montebelli, R. Lowe, I. Ieropoulos, C. Melhuish, J. Greenman, T. Ziemke, in: Proceedings of the Alife XII Conference, Odense, Denmark, 2010.
[29] A.P. Borole, D. Aaron, C.Y. Hamilton, C. Tsouris, Environmental Science & Technology 44 (2010) 2740–2745.
[30] A.K. Manohar, O. Bretschger, K.H. Nealson, F. Mansfeld, Bioelectrochemistry 72 (2008) 149–154.
[31] F. Zhao, R.C.T. Slade, J.R. Varcoe, Chemical Society Reviews 38 (2009) 1926–1939.
[32] N.E. Stein, H.M.V. Hamelers, G. van Straten, K.J. Keesman, Journal of Process Control 22 (2012) 1755–1761.

[33] J.R. Kim, G.C. Premier, F.R. Hawkes, R.M. Dinsdale, A.J. Guwy, Journal of Power Sources 187 (2009) 393–399.
[34] L. Ljung, System Identification: Theory for the User, second ed., Prentice Hall PTR, 1999.
[35] L. Ljung, System Identification Toolbox™ User's Guide, The MathWorks, Inc, Natick, MA, 2012.
[36] P.-Y. Zhang, Z.-L. Liu, Journal of Power Sources 195 (2010) 8013–8018.
[37] W.J. Rugh, J.S. Shamma, Automatica 36 (2000) 1401–1425.
[38] K.Y. Cheng, G. Ho, R. Cord-Ruwisch, Environmental Science & Technology 42 (2008) 3828–3834.
[39] J.R. Kim, J. Rodriguez, F.R. Hawkes, R.M. Dinsdale, A.J. Guwy, G.C. Premier, Energy & Environmental Science 4 (2011) 459–465.
[40] B.E. Logan, J.M. Regan, Trends in Microbiology 14 (2006) 512–518.
[41] H. Richter, K.P. Nevin, H. Jia, D.A. Lowy, D.R. Lovley, L.M. Tender, Energy & Environmental Science 2 (2009) 506–516.
[42] P.S. Bonanni, G.D. Schrott, L. Robuschi, J.P. Busalmen, Energy & Environmental Science 5 (2012) 6188–6195.